JOURNAL OF VIROLOGY, July 2001, p. 6070–6085 Vol. 75, No. 13
0022-538X/01/$04.00+0 DOI: 10.1128/JVI.75.13.6070–6085.2001

Hantavirus Infection Induces the Expression of RANTES and IP-10 without Causing Increased Permeability in Human Lung Microvascular Endothelial Cells

J. BRUCE SUNDSTROM,[1]* LAURA K. MCMULLAN,[2] CHRISTINA F. SPIROPOULOU,[2] W. CRAIG HOOPER,[3] AFTAB A. ANSARI,[1] CLARENCE J. PETERS,[2]† AND PIERRE E. ROLLIN[2]

Department of Pathology and Laboratory Medicine, Emory University School of Medicine, Atlanta, Georgia 30323,[1] and Special Pathogens Branch[2] and Division of AIDS, STD, and TB Laboratory Research,[3] National Center for Infectious Diseases, Centers for Disease Control and Prevention, Atlanta, Georgia 30333

Received 12 December 2000/Accepted 28 March 2001

Sin Nombre virus (SNV) and Hantaan virus (HTN) infect endothelial cells and are associated with different patterns of increased vascular permeability during human disease. It is thought that such patterns of increased vascular permeability are a consequence of endothelial activation and subsequent dysfunction mediated by differential immune responses to hantavirus infection. In this study, the ability of hantavirus to directly induce activation of human lung microvascular endothelial cells (HMVEC-Ls) was examined. No virus-specific modulation in the constitutive or cytokine-induced expression of cellular adhesion molecules (CD40, CD54, CD61, CD62E, CD62P, CD106, and major histocompatibility complex classes I and II) or in cytokines and chemokines (eotaxin, tumor necrosis factor alpha, interleukin 1β [IL-1β], IL-6, IL-8, MCP-1, MIP-1α, and MIP-1β) was detected at either the protein or message level in hantavirus-infected HMVEC-Ls. Furthermore, no virus-specific enhancement of paracellular or transcellular permeability or changes in the organization and distribution of endothelial intercellular junctional proteins was observed. However, infection with either HTN or SNV resulted in detectable levels of the chemokines RANTES and IP-10 (the 10-kDa interferon-inducible protein) in HMVEC-Ls within 72 h and was associated with nuclear translocation of interferon regulatory factor 3 (IRF-3) and IRF-7. Gamma interferon (IFN-γ)-induced expression of RANTES and IP-10 could also be detected in uninfected HMVEC-Ls and was associated with nuclear translocation of IRF-1 and IRF-3. Treatment of hantavirus-infected HMVEC-Ls with IFN-γ for 24 h resulted in a synergistic enhancement in the expression of both RANTES and IP-10 and was associated with nuclear translocation of IRF-1, IRF-3, IRF-7, and NF-κB p65. These results reveal a possible mechanism by which hantavirus infection and a TH1 immune response can cooperate to synergistically enhance chemokine expression by HMVEC-Ls and trigger immune-mediated increases in vascular permeability.

Sin Nombre virus (SNV) has been identified as the etiologic agent responsible for hantavirus pulmonary syndrome (HPS) (37). SNV is a member of the *Bunyaviridae* family of trisegmented negative-sense viruses and is serologically and genetically similar to Hantaan virus (HTN), the virus associated with hemorrhagic fever with renal syndrome (HFRS). Both SNV and HTN primarily infect endothelial cells without causing apparent cytopathic effects (49), and it has been reported that both SNV and HTN use a common receptor, the β3 integrin (CD61) (14, 15), for cellular entry. Infection with hantavirus leads to the generation of antigen-specific activated T cells in primary and secondary lymphoid organs, and there is evidence that in both HPS and HFRS, hantavirus antigen-specific cellular and humoral responses to hantaviral antigens develop during the incubation phase and are present at the clinical onset of HPS (39). These observations and the fact that hantavirus infection by itself does not cause any detectable cytopathic disruption of the vascular endothelium have provided support for a role for immune-mediated mechanisms in the pathogenesis of HPS and HFRS, particularly in the induction of increased vascular permeability in HPS. However, it cannot be concluded that the morbid vascular permeability associated with hantavirus-induced disease is due exclusively to immune-mediated mechanisms without examining the direct effects of hantavirus infection on endothelial cell activation and vascular permeability.

The vascular endothelium responds to environmental and proinflammatory activation signals to influence and direct immune responses (12). Such responses result in the local expression of cytokines and chemokines and of cellular adhesion molecules (CAMs) that assist in the recruitment of circulating immunocytes to areas of injury, inflammation, or viral infection by facilitating the adhesion to and transmigration through activated endothelium. Contact-dependent interactions between leukocytes and the activated endothelium have also been shown to induce changes in endothelial intercellular junctions and associated increases in paracellular permeability of the vascular endothelium (32). Viral infections can also exert changes in the vascular endothelium in a variety of ways, such as inducing endothelial cell activation indirectly by infecting and activating leukocytes and triggering the synthesis and local release of proinflammatory lymphokines (1) or by directly inducing changes in endothelial cell expression of cytokines, che-

* Corresponding author. Mailing address: Department of Pathology and Laboratory Medicine, Winship Cancer Institute, Room B4337, Emory University School of Medicine, Atlanta, GA 30322. Phone: (404) 778-4564. Fax (404) 778-5016. E-mail: JSUNDST@emory.edu.

† Present address: Department of Pathology, University of Texas Medical Branch, Galveston, TX 77555.

mokines, and CAMs in the absence of immune mediators (20, 44, 46). Despite a recent report of experimental infection of bronchial alveolar macrophages with SNV in vitro (26), there is limited evidence that SNV or HTN can infect or activate monocytes and lymphocytes. Therefore, we tested the hypothesis that hantavirus infection directly induces the activation of primary cultures of human microvascular endothelial cells (HMVECs).

Our findings show that SNV and HTN are both able to infect pulmonary HMVECs (HMVEC-Ls) in vitro without affecting detectable levels of the constitutive or (cytokine-) induced expression of endothelial CAMs and do not mediate detectable enhancement of leukocyte adhesion. However, both infection with hantavirus and pretreatment with gamma interferon (IFN-γ) induced the expression of the beta chemokine RANTES and the alpha chemokine IP-10 (the 10-kDa interferon-inducible protein) by HMVEC-Ls. Furthermore, the combination of hantavirus infection and IFN-γ pretreatment resulted in a synergistic enhancement of chemokine expression at both the message and protein levels and was associated with the nuclear translocation of NF-κB p65, interferon regulatory factor 1 (IRF-1), IRF-3, and IRF-7 transcription factors. This selective induction of chemokine synthesis was not associated with any detectable increases in paracellular or transcellular permeability in confluent monolayers of hantavirus-infected HMVEC-Ls or with the loss of the ability of HMVEC-Ls to form functional adherens junctions and permeability barriers. These findings suggest that cellular immune mechanisms may play a more significant role than the direct effects of hantavirus infection in the pathogenesis of increased vascular permeability associated with HPS.

MATERIALS AND METHODS

Cell culture. Primary cultures of HMVEC-Ls isolated from individual donors were obtained cryopreserved at passage 4 (P4) from Clonetics Corporation (Walkersville, Md.). HMVEC-Ls were certified for their homogeneity and characterized as testing positive for expression of acetylated low-density lipoprotein scavenger receptors, von Willebrand factor VIII, and platelet endothelial cell adhesion molecule (PECAM) at P4 by Clonetics. The cells were seeded into tissue culture flasks (5,000 cells/cm^2) or into multiwell plates or onto glass coverslips (10,000 cells/cm^2) precoated with 0.2% gelatin (Sigma, St. Louis, Mo.). Cells were cultured at 37°C in an atmosphere of 5% CO_2 in EGM-2MV growth medium (Clonetics) consisting of modified EGM basal medium supplemented with human recombinant epidermal growth factor (10 ng/ml), hydrocortisone (1 μg/ml), gentamicin (50 μg/ml), amphotericin B (50 μg/ml), bovine brain extract (3 μg/ml), and fetal bovine serum (5%, vol/vol). All experiments were performed at P5 to P8. Additional control experiments performed to characterize and compare the levels of expression of selected endothelial cell-specific antigens (CD62E, vascular-endothelial cadherin, zona occludens 1 [ZO-1], CD31, and von Willebrand factor) or endothelial cell-specific functional activities (e.g., uptake of acetylated forms of low-density lipoprotein, cobblestone morphology of confluent monolayers, and spontaneous capillary-like tubule formation on collagen gels) supported the observation that the primary HMVEC-Ls remained functionally and phenotypically stable at P3 through P11 (data not shown). For some experiments, confluent cultures of HMVEC-Ls were switched to maintenance medium consisting of endothelial basal medium (EBM) basal medium with 5% fetal bovine serum, 20 mM L-glutamine, and gentamicin.

Virus infection. Virus stock pools (VSPs) of SNV and HTN were prepared in Vero E6 cells from prototype strains 9302702 and 76-118 (37), respectively, and then stored in 1-ml aliquots in liquid nitrogen. SNV and HTN VSPs contained approximately 3.0×10^5 50% tissue culture infective doses ($TCID_{50}$) per ml as determined by infection of Vero E6 cells. Mock SNV or HTN controls were prepared by subjecting SNV and HTN VSPs to gamma radiation (5×10^4 Gy). In some experiments, mock Vero controls, prepared by subjecting uninfected Vero cell to gamma radiation (5×10^4 Gy), were included. For all infections, virus was allowed to adsorb to HMVEC-Ls at a multiplicity of infection of approximately 0.1 in serum-free EBM medium with continuous rocking for 60 to 90 min at 37°C. The cells were then washed and afterwards refed and maintained with EBM maintenance medium

Detection of CAMs by EIA. Measurements of the level of expression of CAMs and costimulatory molecules (CSMs) on the HMVEC-L plasma membrane were performed by a variation of the indirect enzyme immunoassay (EIA) method previously described (2). Briefly, HMVEC-Ls were seeded at a concentration of approximately 16,000 cells/ml in a volume of 0.2 ml into individual wells of 96-well tissue culture plates precoated with 0.2% (vol/wt) gelatin (Sigma) in 0.01 M phosphate-buffered saline (PBS), pH 7.2. The HMVEC-Ls were grown to confluence (2 to 3 days) in EGM-2MV; then the medium was replaced with EBM maintenance medium, and the cells were allowed to adjust for another 24 to 48 h. For cytokine-mediated induction, recombinant human cytokines or soluble inducers were added directly to quadruplicate wells in previously defined amounts, yielding a final effective concentration for optimal endothelial cell activation. To assess virally induced CAM expression, endothelial cells were infected with the appropriate VSPs or mock controls as described above. Indirect EIA measurements for CAM expression were performed at various time points postinduction in the following manner. Medium was removed from individual wells and then replaced with fresh medium containing primary antibody diluted at a previously defined optimal concentration (Table 1). The plates were sequentially incubated for 30 min at 4°C, washed twice with ice-cold PBS to remove residual unbound antibody before fixation with 2% paraformaldehyde, washed twice with 0.01 M PBS (pH 7.2) with 0.1% Tween 20 (PBS-Tween), and then treated with blocking buffer containing horse serum (0.5%, vol/vol). Biotinylated horse anti-mouse immunoglobulin (Ig) (Vector Laboratories, Burlingame, Calif.) diluted 1:200 in PBS-Tween was added in a volume of 0.1 ml to each well, and the plates were incubated for an additional 30 min at room temperature (RT). The plates were then washed twice with PBS before the addition of a 1:1,000 dilution of streptavidin-HRP40 (Research Diagnostics Inc., Flanders, N.J.). The plates were incubated for 30 min at RT and washed twice with PBS before the addition of 2,2′-azino-bis(3-ethylbenzothiazoline-6-sulfonic acid (ABTS) peroxidase substrate. Optical density measurements at 409 nm were read on a Dynatech microplate spectrophotometer.

RPA. Total HMVEC-L RNA was extracted from each experimental group using Tri-Pure reagent (Boehringer Mannheim Biochemicals, Indianapolis, Ind.) according to the manufacturer's instructions and then stored in RNase-free water at −70°C until assayed. Measurements of HMVEC-L cytokine and chemokine transcripts were then determined using a RiboQuant MultiProbe RNase protection system (PharMingen, San Diego, Calif.) following instructions provided by the manufacturer and as previously described (22). Comparisons of the levels of mRNA expression between samples were made using a Bio-Rad (Hercules, Calif.) model GS-525 storage phosphorimaging system with molecular analyst software. The values obtained for each level of chemokine mRNA measured were normalized against the combined levels of expression obtained for mRNA from L32 and GAPDH (glyceraldehyde-3-phosphate dehydrogenase) housekeeping genes loaded within the same lane on the RNase protection assay (RPA) gel.

Detection of chemokines and cytokines by enzyme-linked immunosorbent assay (ELISA). The induction of chemokines and cytokines in virally infected or cytokine-pretreated endothelial cells was detected by QuantiKine quantitative sandwich EIAs (R&D Systems, Minneapolis, Minn.) according to the manufacturer's instructions.

Immunofluorescence of nuclear transcription factors and endothelial intercellular junctions. HMVEC-Ls were grown to confluence on gelatin-coated glass coverslips and then experimentally treated and fixed with a solution of 95% ethanol and 5% acetic acid. Fixed specimens were washed three times in saponin wash buffer consisting of 0.1% (wt/vol) saponin (Sigma) in 0.01 M PBS, pH 7.4, with Ca^{2+} and Mg^{2+}. The fixed and permeabilized specimens were then blocked for 30 min at RT with saponin wash buffer containing 5% (vol/vol) normal goat serum. Next, the specimens were incubated with the appropriate primary antibodies (Table 1) diluted 1:10 in saponin wash buffer for 30 to 60 min at RT. Unbound primary antibody was removed by three washes with saponin wash buffer. Bound primary antibody was developed by adding an appropriate secondary fluorescent-antibody conjugate diluted 1:1,000 in saponin wash buffer followed by incubation for an additional 30 min with gentle rotation. Unbound fluorescent antibody conjugate was removed by washing three times with saponin wash buffer. Immunostained specimens were then preserved with a drop of VectaShield (Vector Laboratories) under a glass coverslip and viewed with a Nikon Eclipse epifluorescent microscope.

Immunoprecipitation and Western blotting of adherens junction complexes. Confluent monolayers of HMVEC-Ls grown in gelatin-coated 25-cm^2 sterile

TABLE 1. Immunoglobulin reagents used for EIA, IFA, immunoprecipitation, and Western blotting[a]

Specificity	Species	Description	Isotype	Source	Clone or catalog no.	Working dilution
P-selectin	Mouse	Primary	IgG1 κ	Zymed, San Francisco, Calif.	WAPS 12.2	3–10 μg/ml
CD40	Mouse	Primary	IgG1 κ	Ancell, Bayport, Minn.	EA-5	1:100
CD62E	Mouse	Primary	IgG1 κ	Ancell	1.2B6	1:100
CD106	Mouse	Primary	IgG1 κ	Ancell	1.G11B1	1:100
CD54	Mouse	Primary	IgG1 κ	Ancell	8.4A6	1:100
CD61	Mouse	Primary	IgG1 κ	PharMingen	F11	0.5 μg/ml
MHC-I	Mouse	Primary	IgG1 κ	Dako, Carpinteria, Calif.	W6.32	1:100
MHC-II	Mouse	Primary	IgG1 κ	Dako	CR3/43	1:100
IRF-1	Rabbit	Primary	IgG	Santa Cruz Biotechnology, Santa Cruz, Calif.		1:200
IRF-3	Rabbit	Primary	IgG	Santa Cruz Biotechnology	SC-9802	1:200
IRF-7	Rabbit	Primary	IgG	Santa Cruz Biotechnology	SC-9803	1:200
NF-κB p65	Rabbit	Primary	IgG	Santa Cruz Biotechnology	SC-109	1:200
ZO-1	Rabbit	Primary	IgG	Zymed	61-7300	1:100
CAd-5	Mouse	Primary	IgG1	ImmunoTech	TEA 1/31	1:100
CD31	Mouse	FITC conjugate	IgG1	Ancell	158-2B3	1:100
Plakoglobin	Mouse	Primary	IgG1 κ	Zymed	13-8500	1:100
rHu-TNE-R–Ig	Human	Primary	NA	Bristol-Meyers Squibb	NA	
Mouse Ig	Goat	FITC conjugate	IgG	PharMingen	12064D	1:100
IgG1	Mouse		IgG1 κ	Dako	Myeloma protein	1:100

[a] NA, not applicable.

tissue culture flasks were washed twice with 0.01 M PBS, pH 7.2, containing Ca^{2+} and Mg^{2+} and then washed twice with serum-free EGM medium. Cell lysates containing membrane-associated adherens junction complexes were prepared by subjecting HMVEC-Ls to gentle rotation for 30 min in a volume of 0.5 ml of ice-cold extraction buffer: Tris-buffered saline, pH 7.5, containing 1 mM phenylmethylsulfonyl fluoride, 40 U of aprotinin/ml, 15 μg of leupeptin/ml, 15 μg of leupeptin/ml, and 1% (vol/vol) Triton X-100. Antibody-coated protein G Sepharose beads were prepared by mixing 60 μl of a 50% (vol/vol) slurry of preequilibrated protein G Sepharose beads in lysis buffer with anti-cadherin 5 (CAD-5) antibody (Table 1) and then adjusting to a final volume of 500 μl in Tris-buffered saline for a final antibody concentration of 2 μg/ml and incubating overnight at 4°C. The antibody-coated Sepharose beads were washed three times in lysis buffer, resuspended in a volume of 500 μl of precleared cell lysate (corresponding to 500,000 to 1,000,000 HMVEC-Ls), and then incubated with gentle rotation for 1 h at RT. The immunoprecipitates were then washed three times with 1 ml of lysis buffer (without Triton X-100), resuspended in a volume of 30 μl of 2× sample loading buffer, and boiled for 5 min. The samples were then resolved on a 7.5% polyacrylamide gel before electrophoretic transfer to a nitrocellulose membrane. Before immunoblotting, the nitrocellulose membranes were immersed in blocking solution and incubated at RT with gentle rotation for 30 min. Afterwards, the blocking solution was replaced with fresh buffer containing (1 μg/ml) antiplakoglobin antibody (Table 1) and incubated overnight at 4°C. The primary antiplakoglobin antibody was detected using a horseradish peroxidase-conjugated secondary reagent and a luminol-based substrate for horseradish peroxidase-catalyzed reactions (NEN Life Science, Boston, Mass.).

Permeability studies. Measurements of paracellular or transcellular permeability were performed on confluent monolayers of uninfected, mock-infected, or hantavirus-infected microvascular endothelial cells. Briefly, HMVEC-Ls were grown to confluence on 12-mm-diameter transwell culture inserts (Millipore). The establishment of permeability barriers in confluent HMVEC-L monolayers was confirmed by transendothelial electrical measurements and by passive diffusion of phenol red (Sigma) as previously described (23). Measurements of endothelial paracellular permeability were determined utilizing fluorescein isothiocyanate (FITC)-conjugated dextran particles (dextran-FITC) with average sizes of 10, 40, and 70 kDa. Dextran-FITC (100 μM) was added in a volume of 300 μl of fresh medium to the apical chamber of triplicate culture inserts. The HMVEC-L cultures were allowed to equilibrate with the dextran-FITC particles for 1 h at 37°C in a 5% CO_2 humidified atmosphere. A volume of 60 μl was then removed from a total volume of 500 μl of medium in the basal chamber and diluted in 1:5 in a 0.1% solution of sodium dodecyl sulfate (SDS) in distilled H_2O. Fluorescence at 488/520 nm was determined using a TECAN (Research Triangle Park, N.Car.) fluorescence microplate reader. To determine transcellular permeability, dextran-FITC particles (3 kDa) were cocultured for 30 min with confluent HMVEC-Ls. The culture inserts were then placed at 4°C, and the medium was replaced. The cultures were then allowed to equilibrate for 1 h at 37°C before fluorescence measurements were made. Titration of dextran-FITC particles in SDS buffer was performed to correlate measured fluorescence with molar concentrations of dextran-FITC. Both transcellular and paracellular permeability flux were expressed as the mean nanomolar dextran concentration per square centimeter (surface area of culture insert) per hour from triplicate cultures.

Statistical analysis. Statistically significant differences in the measurements of CAM, cytokine, and chemokine expression between control and virally infected groups were determined by one-way analysis of variance followed by Student's *t* tests for comparisons between individual experimental groups. The results presented herein are representative of a minimum of three repeats of each assay performed regardless of whether the data obtained were negative (no effect) or positive.

RESULTS

Susceptibility of HMVEC-Ls to hantavirus infection. Since the pathogenesis of HPS is primarily targeted to the lung and the virus has been shown to be present within the microvascular endothelial cells, HMVEC-Ls were chosen for the studies described in this report. Although experimental infection of endothelial cells in vitro with hantavirus has been previously reported (38, 47), we established the susceptibility of our primary HMVEC-Ls to infection with the defined SNV and HTN strains used in this study. Both SNV and HTN nucleocapsid proteins (NP) were readily detectable by immunofluorescence assay (IFA) by 24 h postinfection (Fig. 1). As expected, hantavirus NP was undetectable in mock-infected HMVEC-Ls (data not shown). To more carefully determine the early events of viral protein expression within the infected endothelial cells, hantavirus NP was immunoprecipitated from [^{35}S]Met-labeled HMVEC-Ls using the cross-reactive monoclone GB04 (Table 1) after infection with both SNV and HTN. Readily detectable levels of hantavirus NP were measured by 24 h with either HTN- or SNV-infected (but not mock-infected) HMVEC-Ls (data not shown), and these levels increased over 96 h. Neither HTN nor SNV causes detectable cytopathic effect in vitro. Therefore, the $TCID_{50}$ for each virus was determined utilizing Vero E6 by immunohistochemistry and the methylcellulose

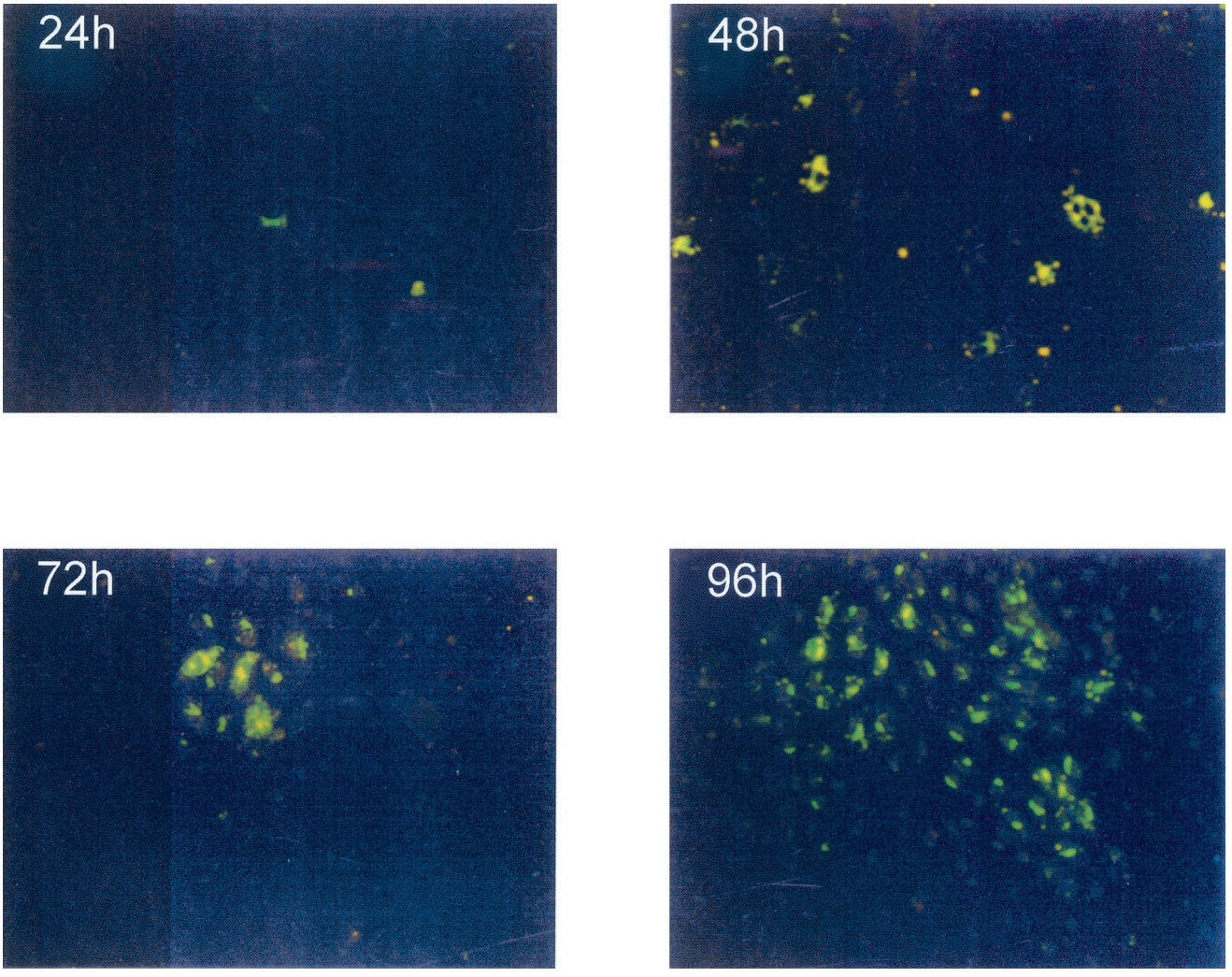

FIG. 1. Indirect immunofluorescence of hantavirus NP in infected HMVEC-Ls. Hantavirus-infected HMVEC-Ls were grown on glass coverslips and then fixed in 10% neutral buffered formalin at the indicated times postinfection. The infected cells were then indirectly immunostained with a rabbit polyclonal antibody which recognizes both SNV NP and HTN NP and then developed with horse anti-rabbit Ig–biotin and streptavidin-FITC. Magnification, ×40.

overlay technique previously described (5). Data obtained indicated that the $TCID_{50}$ for the prepared hantavirus stock pools was approximately 3×10^5/ml.

Effects of proinflammatory cytokines and hantavirus infection on CAM expression by HMVEC-Ls. The constitutive and cytokine-induced expression of adhesion and CSMs from the selectin family (CD62E and CD62P), the integrin family (CD61), and the Ig supergene family (CD40, CD106, CD54, major histocompatibility complex class I [MHC-I], and MHC-II) was measured on resting confluent cultures of HMVEC-Ls. HMVEC-Ls (in vitro) constitutively express high levels of MHC-I, moderate levels of CD40, CD54, and CD61, and low to undetectable levels of CD62P, CD106, CD62E, and MHC-II. The results in Fig. 2A are presented with IgG1 isotype control optical density values subtracted. To establish the (cytokine-) induced profile of CAM and CSM expression on HMVEC-Ls, indirect EIA measurements were made after induction for 6, 24, and 48 h with a cocktail of IFN-γ (1,000 U/ml) and tumor necrosis factor alpha (TNF-α) (10 ng/ml) (Fig. 2A). There was a marked sustained increase of high levels of CD40, CD54, and CD106 within 24 h. A transient increase in the expression of CD62E was observed within 6 h that decreased to basal levels by 24 h (in the presence of cytokines). There was a slight increase in the level of CD62P and a steady increase in expression of MHC-II after 24 h that continued to rise to moderate levels at 48 h.

The effects of hantavirus infection on the constitutive or cytokine (TNF-α, 10 ng/ml for 6 h)-induced expression of CAMs by HMVEC-Ls was measured by indirect EIA. No detectable changes in the constitutive and cytokine-induced patterns of CAM expression were seen in hantavirus-infected HMVEC-L cultures at 6, 24, 48, or 96 h postinfection by either EIA or flow microfluorometry (data not shown). Likewise, no significant virus-specific changes in the transcription of vascular CAM 1 (VCAM-1), intercellular CAM 1 (ICAM-1), or E-selectin genes were detected by RPA despite low background levels of VCAM-1 gene expression and a transient expression of E-selectin. at 6 h in all experimental groups (Fig.

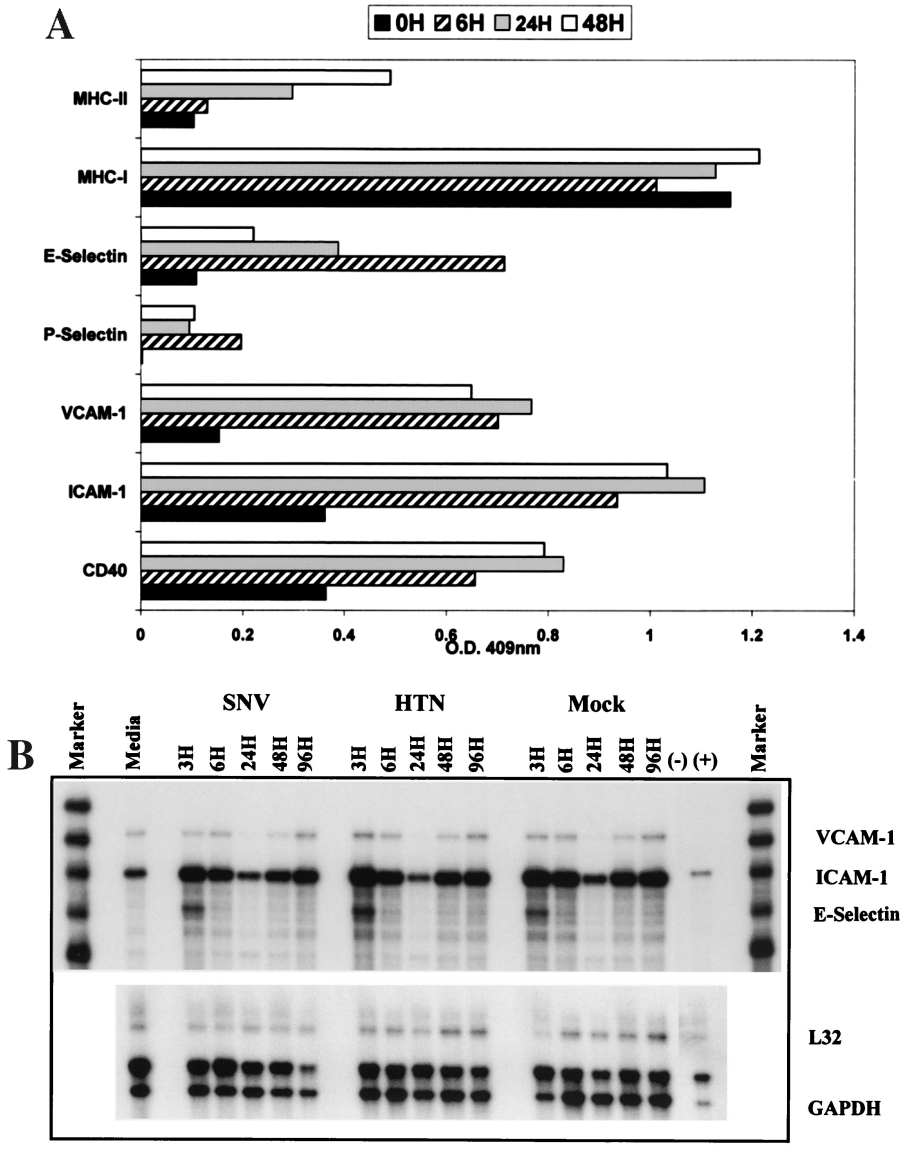

FIG. 2. Measurement of constitutive and induced expression of CAMs by HMVEC-L. (A) HMVEC-Ls were seeded and grown to confluence in gelatin-coated 96-well tissue culture plates. Triplicate wells were then treated with a combination of recombinant human TNF-α (10 ng/ml) and IFN-γ (1,000 U/ml) for 6, 24, and 48 h. Replicate wells were incubated with CAM-specific monoclonal antibodies (Table 1), fixed with 2% paraformaldehyde, and developed with an anti-mouse Ig peroxidase conjugate and ABTS substrate. CAM expression is shown as optical density (O.D.). The results are representative of three separate experiments. (B) HMVEC-Ls grown to confluence in tissue culture were infected with SNV, HTN, or mock virus or left uninfected; cellular RNA was extracted at the indicated times postinfection. Total mRNA for each CAM was then quantitated by RPA as described in the text. GAPDH controls were used to confirm equal loading of mRNA samples among separate lanes in an acrylamide sequencing gel. The ^{32}P-labeled gels were then exposed on photographic film for 24 h for VCAM-1, ICAM-1, or E-selectin mRNA or for 6 h for GAPDH gene expression. The results are representative of three separate experiments. (C) Quantitative densitometric measurements of CAM and GAPDH gene expression for each of the treatment groups were determined as described in the text. Values for CAM gene expression shown in panel B are presented here as the percentage of the GAPDH gene expressed in the same lane. The transient hybridization of the GAPDH gene to its labeled probe is a normal occurrence in the RiboQuant assay that results in two bands (BD PharMingen Technical Service, personal communication). The lower-molecular-weight GAPDH band was used to determine GAPDH gene expression. Less-than-threefold differences in the levels of CAM gene expression between treatment groups were not considered significant. (D) HMVEC-Ls grown to confluence in tissue culture were infected with SNV, HTN or mock virus or left uninfected for the indicated times and then treated with recombinant human TNF-α for 6 h. RPA was then performed exactly as described for panel B. (E) Quantitative densitometric measurements of CAM and GAPDH gene expression for each of the treatment groups were determined as described in the text. Values for CAM gene expression shown in panel B are presented here as the percentage of the GAPDH gene expressed in the same lane.

2B and C). This failure to detect virus-specific changes in CAM expression was not due to technical issues, since TNF-α-induced changes were readily observed. Furthermore, no significant hantavirus-specific modulation in cytokine-induced CAM gene expression by HMVEC-Ls was observed (Fig. 2D and E). Thus, even though a broad range of (cytokine-) induced changes was observed in the expression of several CAMs on HMVEC-Ls at both the protein and message levels, no mod-

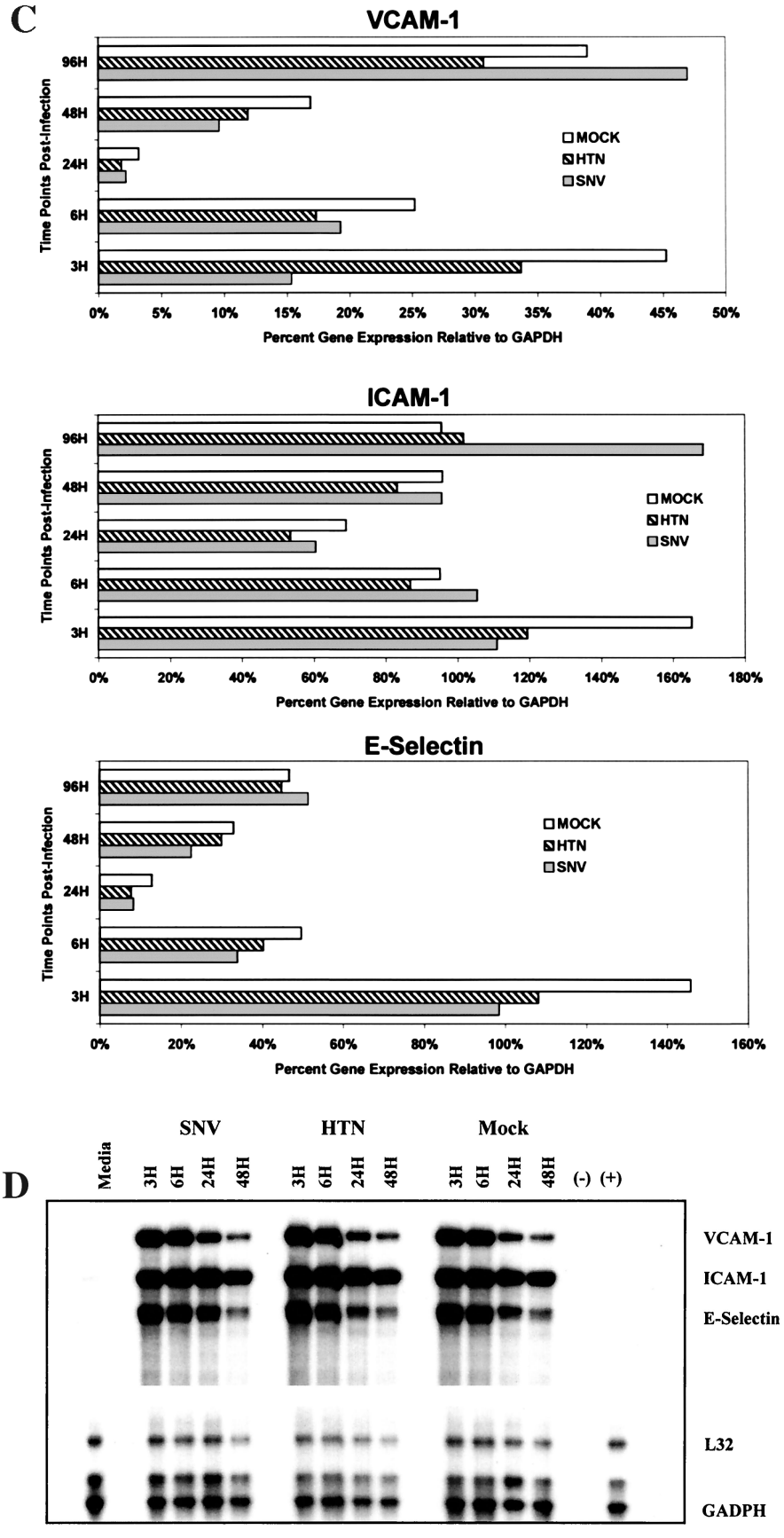

FIG. 2—*Continued.*

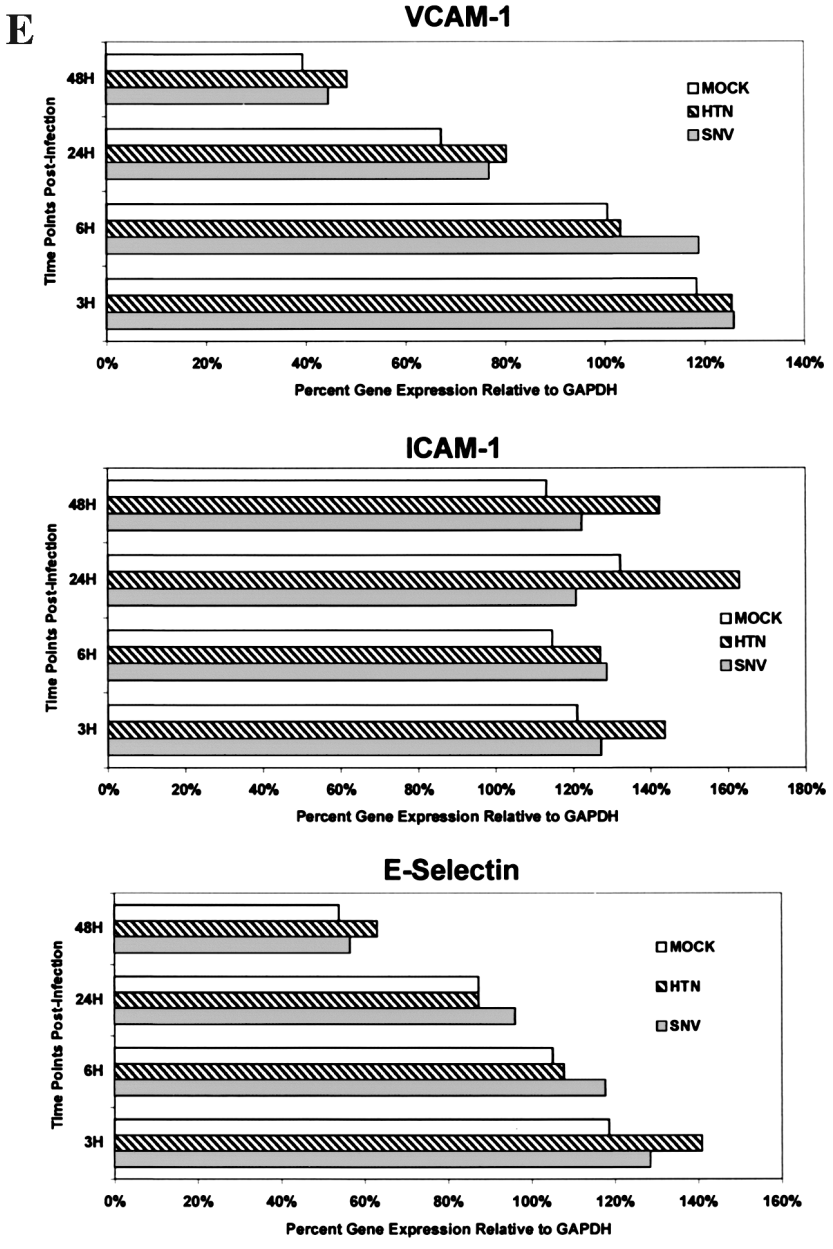

FIG. 2—*Continued.*

ulation in the constitutive or (cytokine-) induced levels of expression of the CAMs was detected in HMVEC-Ls infected with either SNV or HTN at any of the time points tested.

Constitutive and (cytokine-) induced chemokine and cytokine expression in uninfected HMVEC-Ls. There are an increasing number of reports describing the considerable differences in the constitutive and induced expression profiles of cytokines, chemokines, and their receptors by endothelial cells derived from different tissue lineages (6, 17, 41). In HPS the microvascular endothelial cells of the lung are heavily infected and the postcapillary venules are the apparent anatomical site of the pathology of this hantavirus-induced disease. Therefore, experiments were conducted to establish the baseline ability of the primary HMVEC-Ls to express cytokines and chemokines in order to more accurately assess the significance of the direct effects of hantavirus infection on the induction of chemokines and cytokines in HMVEC-Ls. The patterns of constitutive and (cytokine-) induced expression of the β-chemokines eotaxin, MIP-1α, MIP-1β, MCP-1, and RANTES, the α-chemokine interleukin 8 (IL-8), and the cytokines TNF-α and IL-6 in HMVEC-Ls were evaluated by capture ELISA (Fig. 3A). HMVEC-Ls were grown to confluence in complete medium as previously described. The medium was replaced with fresh complete medium alone (constitutive expression) or with medium containing IFN-γ (2,000 U/ml), TNF-α (10 ng/ml), IFN-γ plus TNF-α (10 ng/ml), or IL-1β (200 U/ml) (induced expression). There were no detectable levels of constitutive expression of eotaxin or TNF-α. Constitutive expression of MIP-1α

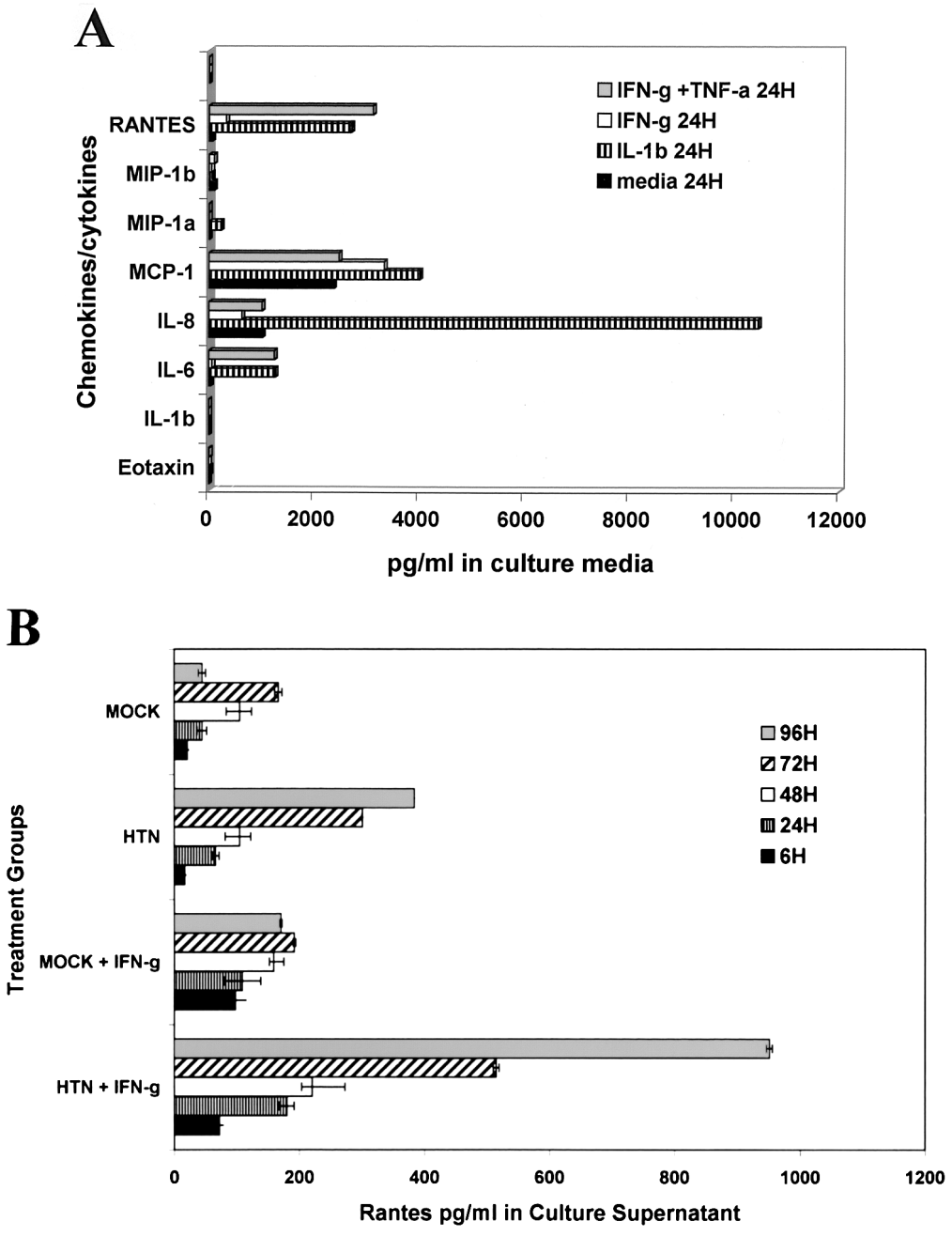

FIG. 3. Constitutive and induced expression of cytokines and chemokines by HMVEC-Ls. (A) HMVEC-Ls were grown to confluence in triplicate cultures and then treated with rHu-IL-1β (1,000 U/ml), rHu-IFN-γ (2,000 U/ml), rHu-TNF-α (10 ng/ml), or IFN-γ plus TNF-α (2,000 U/ml) for 6, 24, and 48 h. The mean concentration of induced cytokines and chemokines in culture supernatant fluids was determined by capture ELISA. The optimal induced response for each chemokine or cytokine is shown. (B) Enhancement of induced expression of RANTES in HMVEC-Ls by the synergistic effects of infection with HTN and treatment with IFN-γ. HMVEC-Ls were treated with IFN-γ for 24 h at 6, 24, 48, 72, and 96 h after infection with HTN or mock infection controls. Mean values, determined by ELISA, for triplicate cultures of HMVEC-Ls are presented.

was barely detectable by ELISA at the picogram-per-milliliter level. IL-6 (32 pg/ml), MIP-1β (64 pg/ml), and RANTES (58 pg/ml) were expressed in moderate levels in culture supernatants, while MCP-1 (589 pg/ml) and IL-8 (1,018 pg/ml) could be detected at nanogram-per-milliliter levels. Treatment with IL-1β resulted in strong induction of IL-6 (1,258 pg/ml), IL-8 (10,461 pg/ml), MCP-1 (7,557 pg/ml), and RANTES (2,710 pg/ml), moderate induction of MIP-1α (223 pg/ml), weak induction of MIP-1β (87 pg/ml), and no induction of TNF-α. Treatment of HMVEC-Ls with a combination of IFN-γ and TNF-α induced strong expression in IL-6 (1,246 pg/ml), IL-8 (1,013 pg/ml), RANTES (3,129 pg/ml), and MIP-1β (731 pg/ml) and no induction of eotaxin, MIP-1α, or TNF-α. Treatment of HMVEC-Ls with IFN-γ induced marked levels of

MCP-1 expression (3,341 pg/ml), moderately increased levels of RANTES expression (328 pg/ml), weakly induced IL-6 (59 pg/ml), and showed no induction of eotaxin, MIP-1α, MIP-1β, or TNF-α.

Synergistic effect of IFN-γ and hantavirus infection on chemokine and cytokine expression in HMVEC-Ls. Triplicate cultures of HMVEC-Ls were left uninfected, mock infected, or infected with SNV or HTN. At 6, 24, 48, 96, and 120 h postinfection, the medium was replaced with complete medium containing recombinant human IFN-γ (rHu-IFN-γ) at 2,000 U/ml. After 24 h the supernatant fluids were collected and assayed by sandwich ELISA for cytokines and chemokines (Fig. 3B), and the cellular RNA was extracted and levels of cytokine and chemokine mRNA were measured by RPA (Fig. 4). A significant hantavirus-mediated synergistic enhancement of IFN-γ-induced expression of RANTES and IP-10 in HMVEC-Ls was observed (Fig. 3B and 4). IFN-γ treatment increased RANTES expression from 45 to 171 pg/ml in the 96-h mock-infected HMVEC-Ls and from 383 to 951 pg/ml in (96-h) HTN-infected HMVEC-Ls. Similar results were also observed with SNV. Thus, hantavirus infection increased the level of RANTES expression approximately ninefold over mock infection, and pretreatment with IFN-γ increased RANTES expression in hantavirus-infected HMVEC-Ls approximately sixfold over that in mock-infected IFN-γ pretreated groups (Fig. 3B). This apparent synergistic enhancement in chemokine expression was also observed at the message levels for both RANTES and IP-10 in hantavirus-infected HMVEC-Ls (Fig. 4).

The fact that the combination of TNF-α and IFN-γ also significantly increased RANTES expression beyond levels of expression measured after treatment with IFN-γ alone in uninfected HMVEC-Ls suggested that the synergistic effects of hantavirus infection and IFN-γ might somehow be mediated through the TNF receptor (TNF-R) signaling pathway. Therefore, HMVEC-Ls were infected with either SNV or HTN and then treated with IFN-γ in the presence of pretitrated doses of soluble TNF-R–Ig fusion protein. TNF-R–Ig did not inhibit the virus-specific enhancement of IFN-γ-induced RANTES expression by HMVEC-Ls but was able to block TNF-α induction of CD62E on HMVEC-Ls (data not shown). TNF-α was also undetectable by ELISA at the picogram-per-milliliter level in culture supernatant fluids of hantavirus-infected HMVEC-Ls (data not shown).

Effect of IFN-γ and hantavirus infection on the nuclear translocation of IRF-3, IRF-7, and NF-κB p65 in HMVEC-Ls. The genes encoding RANTES and IP-10 are located on the human chromosomes 17q11.2 (11) and 4q21 (33), respectively. Regulation of gene transcription of both chemokines involves the binding of nuclear transcription factors to unique IFN-stimulated response element (ISRE) and NF-κB binding sites located in the RANTES and IP-10 gene promoters. The nuclear transcription factors IRF-1, IRF-3, IRF-7, and NF-κB p65 have all been reported to be involved in the regulation of cytokine or virus-induced gene expression of these chemokines (16, 28, 30, 34). Therefore, we chose to examine the patterns of nuclear translocation of IRF-1, IRF-3, IRF-7, and NF-κB p65 in uninfected or hantavirus-infected HMVEC-Ls with and without IFN-γ pretreatment using direct immunofluorescence. Uninfected HMVEC-Ls did not show detectable levels of nuclear IRF-1, IRF-3, IRF-7, or NF-κB p65 (Fig. 5O to R), indicating no constitutive activation. Pretreatment of uninfected HMVEC-Ls with poly(I · C), a synthetic double-stranded RNA copolymer of inosinic and cytidylic acids, induced nuclear translocation of IRF-3 and IRF-7 (Fig. 5F and G). However, IRF-1 and NF-κB p65 could not be detected in the nucleus by IFA after treatment with poly(I · C) (Fig. 5E and H). Nuclear translocation of NF-κB p65 was achieved after pretreatment with TNF-α, a strong inducer of NF-κB (Fig. 5I).

As we have previously demonstrated, RANTES can be induced in HMVEC-Ls by IFN-γ (Fig. 3B and 4)). When uninfected HMVEC-Ls were pretreated with IFN-γ, IRF-1 and IRF-3 (Fig. 5A and B) but not IRF-7 or p65 (Fig. 5C and D) could be detected in the nucleus. Hantavirus infection of HMVEC-Ls, which also induced RANTES and IP-10 gene expression, caused nuclear translocation of both IRF-3 and IRF-7 (Fig. 5K and L) but not IRF-1 or p65 (Fig. 5J and M). Pretreatment of hantavirus-infected HMVEC-Ls with IFN-γ, which led to enhanced gene expression of both RANTES and IP-10 (Fig. 3B and 4), resulted in the nuclear translocation of IRF-1, IRF-3, IRF-7 (data not shown), and NF-κB p65 (Fig. 5N), thus suggesting a role for all four of these transcription factors in the observed enhancement of chemokine gene expression by HMVEC-Ls. Dual staining for both IRF3 and IRF7 and for hantavirus NP (Fig. 5K and L) revealed nuclear translocation of IRF-3 and IRF-7 occurring in both infected (NP^+) and uninfected (NP^-) cells. These findings suggest that chemokine expression may be indirectly induced in uninfected neighbor cells through the actions of virus-induced soluble mediators.

Permeability studies. The effect of hantavirus infection on mediating changes in endothelial permeability was assessed both by characterization of the constitutive and virus-induced profiles of the organization and distribution of integral proteins involved in endothelial intercellular junctions and by functional permeability assays utilizing passive diffusion of molecule-sized dextran-FITC particles.

(i) Effect of hantavirus infection on endothelial intercellular junctions. HMVEC-Ls were grown to confluence on glass coverslips and then left uninfected, mock infected, or infected with hantavirus. At day 7 postinfection the HMVEC-Ls were fixed and immunostained with antibodies to ZO-1, to characterize occludens (or tight) junctions (Fig. 6A, panels A, D, G, and J), CAD-5, to characterize adherens junctions (Fig. 6A, panels B, E, H, and K), CD31 or PECAM (Fig. 6A, panels C, F, I, and L), and hantavirus NP (Fig. 6A, panels A, B, and C). No detectable hantavirus-specific effects were observed in the organization or distribution of the integral intercellular junctional proteins in the absence of soluble mediators of paracellular permeability. Treatment of uninfected HMVEC-Ls with recombinant human TNF-α (10 ng/ml) for 24 h resulted in a dramatic disruption in the intercellular organization of ZO-1, CAD-5, and CD31 (Fig. 6A, panels K, L, and M). Treatment of uninfected HMVEC-Ls with recombinant IFN-γ or RANTES (1,000 U/ml) for the same period showed no effect on the organization and distribution of endothelial intercellular junctional proteins by IFA (data not shown).

(ii) Effect of hantavirus infection on HMVEC-L paracellular or transcellular permeability to fluorescent dextran particles. The strength and integrity of endothelial intercellular junctions

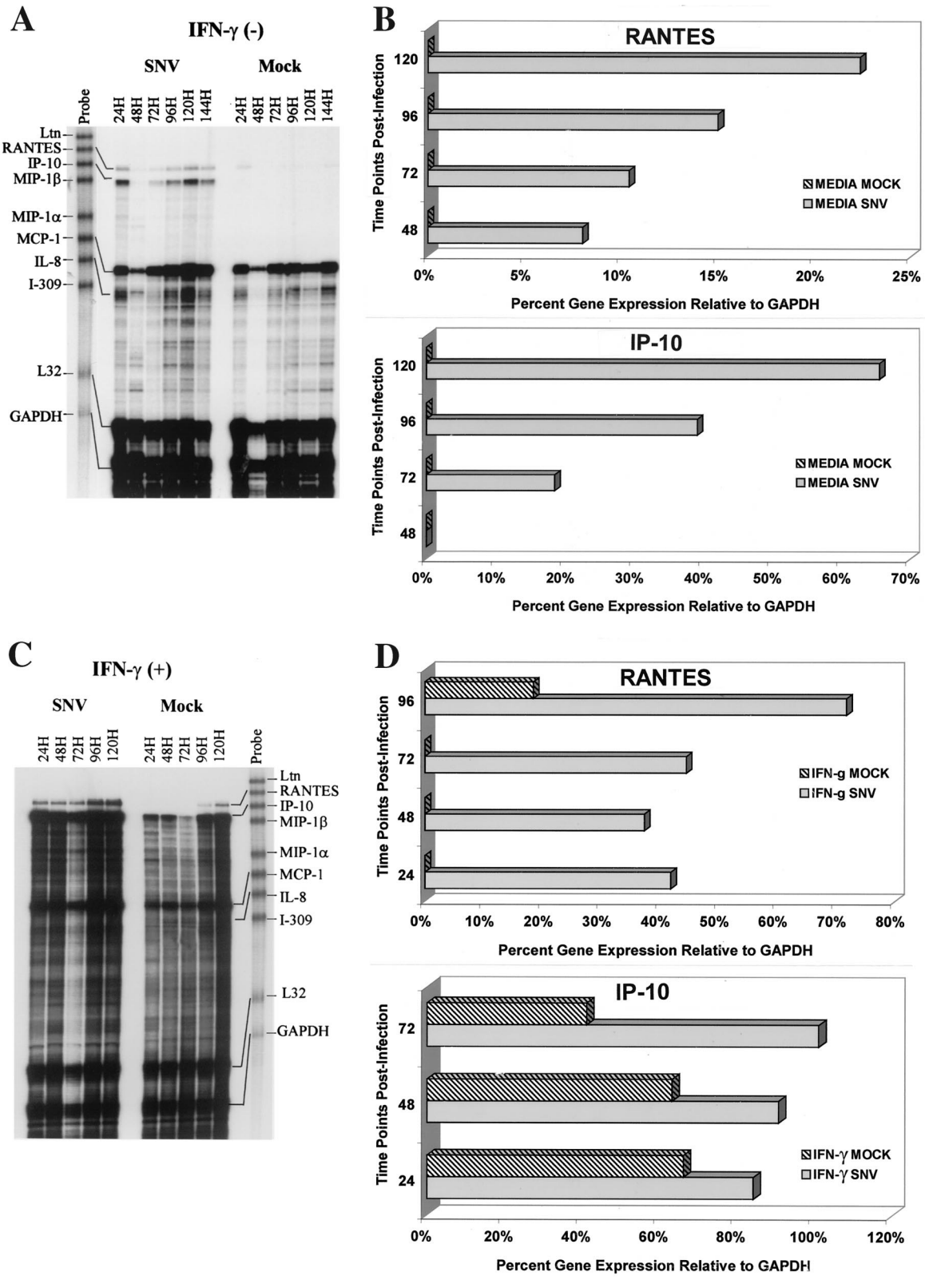

FIG. 4. Synergistic effects of hantavirus infection and IFN-γ on RANTES and IP-10 gene expression by HMVEC-Ls. Measurements of SNV-specific induction of IP-10 and RANTES mRNA in HMVEC-Ls before (A) and after (C) treatment with IFN-γ (1,000 U/ml, 24 h) were determined by RPA at the indicated time points postinfection as described in the text and for Fig. 2. Quantitative densitometric measurements of IP-10, RANTES, and GAPDH gene expression for each of the treatment groups before (B) and after (D) treatment with IFN-γ (1,000 U/ml, 24 h) were determined as described in the text and for Fig. 2. Values for IP-10 and RANTES gene expression are the percentages of the GAPDH gene expressed in the same lane.

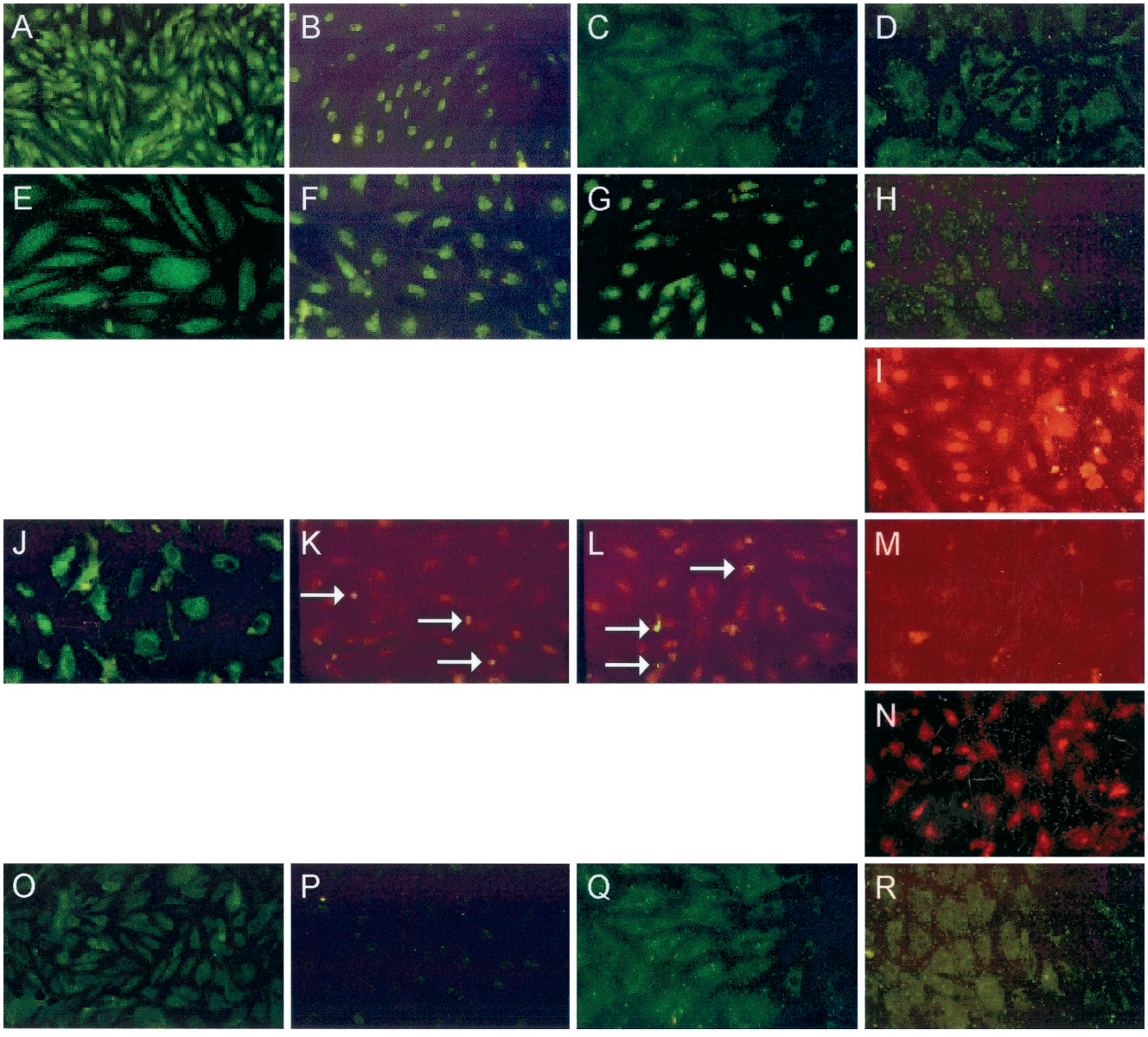

FIG. 5. Patterns of nuclear translocation of IRF-1, IRF-3, IRF-7, or NF-κB p65 by IFA in HMVEC-Ls after hantavirus infection or cytokine treatment. The cellular distributions of nuclear transcription factors in HMVEC-Ls before and after induction and/or activation by virus or by specific inducers were delineated by IFA. The absence of nuclear translocation is characterized by the dark, hollow appearance of nuclei in HMVEC-Ls. The cellular localization of the following proteins is shown: IRF-1 in HMVEC-Ls pretreated with IFN-γ for 24 h (A) and with poly(I · C) for 24 h (E), in HMVEC-Ls treated at day 7 after infection with HTN (J), and in uninfected HMVEC-Ls (O); IRF-3 in HMVEC-Ls pretreated with IFN-γ for 24 h (B) and with poly(I · C) for 24 h (F), in HMVEC-Ls at day 7 after infection with HTN (dually stained for IRF-7 and hantavirus NP [white arrows]) (K), and in uninfected HMVEC-Ls (P); IRF-7 in HMVEC-Ls pretreated with IFN-γ for 24 h (C) and with poly(I · C) for 24 h (G), in HMVEC-Ls at day 7 after infection with HTN (dually stained for IRF-7 and hantavirus NP [white arrows]) (L), and in uninfected HMVEC-Ls (Q); and NF-κB p65 in HMVEC-Ls pretreated with IFN-γ for 24 h (D), with poly(I · C) for 24 h (H), and with TNF-α for 6 h (I), in HMVEC-Ls at day 7 after infection with HTN (M) and at day 7 after infection with SNV after 24 h of pretreatment with IFN-γ (N), and in uninfected HMVEC-Ls (R).

limits the diffusion or permeability of small molecules at endothelial intercellular borders. It was reasoned that hantavirus infection of confluent cultures of HMVEC-Ls may have subtle effects that would result only in selective increases in permeability to molecules of a particular size. To assess the functional effects of hantavirus infection on paracellular permeability, passive diffusion of 10-, 40-, or 70-kDa fluorescent dextran particles was measured in confluent cultures of hantavirus-infected, mock-infected, or uninfected HMVEC-Ls grown on transwell culture inserts as described in Materials and Methods. The paracellular flux, measured as the nanomolar concentration of dextran-FITC per square centimeter per hour, was roughly inversely proportional to the average size of the dextran particle. No detectable virus-specific changes in permeability were observed (Fig. 5B). Virus-induced changes in transcellular permeability were measured by passive diffusion of

3-kDa dextran-FITC as described in Materials and Methods. Again, no virus-specific changes in (transcellular) permeability were observed (Fig. 5B).

(iii) Effect of hantavirus infection on the ability of HMVEC-Ls to form functional adherens junctions. The plasticity of the vascular endothelium allows responses to proinflammatory or environmental signals to occur locally, transiently, and reversibly. Therefore, we tested whether hantavirus infection would compromise the ability of confluent monolayers of HMVEC-Ls to reestablish functional adherens junctions after the experimental disruption of the endothelial permeability barrier. The endothelial adherens complex is comprised of an integral transmembrane protein, vascular endothelial cadherin (CAD-5), which is affiliated with a number of intracytoplasmic adapter molecules, the catenins (10). In the mature functional adherens complex, CAD-5 forms Ca^{2+}-dependent homodimeric complexes with the extracellular domains of CAD-5 proteins on adjacent cells. This association initiates the assembly of the adherens junction complex with the addition of intracytoplasmic α-, β-, and γ-catenins. Plakoglobin, or γ-catenin, is one of the last adapter molecules to join the adherens complex and is also one of the first to disassociate from the disrupted complex (9). To establish the dynamics of the formation of the adherens complex in confluent HMVEC-Ls, we tested the response of HMVEC-Ls to experimental disruption by exposure to EDTA. After HMVEC-Ls were treated with different concentrations of EDTA for different exposure periods, cell lysates were prepared immediately or after the cells had been allowed to recover in complete medium. Afterwards, immunoprecipitation was performed with antibodies directed against human CAD-5, and the presence of plakoglobin by was confirmed by Western blotting as described in Materials and Methods. Complete disruption of the adherens junction complex in confluent HMVEC-Ls, achieved after treatment for 1 min with 50 mM EDTA, was completely reversed after a 60-min recovery period in complete medium (Fig. 6C).

Under the same experimental conditions, we examined the effect of hantavirus infection on the ability of HMVEC-Ls to form adherens junctions and establish a functional permeability barrier. HMVEC-Ls were grown to confluence on transwell filters, and the determination of functional barrier functions was established by the phenol red technique as described in Materials and Methods (23). Endothelial cells were infected with hantavirus, mock infected, or left uninfected. At day 7 postinfection, the ability of HMVEC-Ls to re-establish functional permeability barriers after experimental disruption with EDTA was assessed using 70-kDa dextran-FITC particles in passive diffusion experiments. No detectable virus-specific effects on the ability of HMVEC-Ls to form functional adherens junctions were observed.

DISCUSSION

A significant finding of this investigation was the observation that hantavirus infection selectively induces expression of the chemokines RANTES and IP-10 in endothelial cells. To our knowledge, this is the first report of hantavirus infection inducing chemokine synthesis by endothelial cells. However, an equally remarkable outcome of our research was the striking absence of activation and lack of response by HMVEC-Ls to infection with SNV or HTN, especially considering the severe vascular disorders associated with HPS and HFRS. In other virally mediated vascular and hemorrhagic diseases, the direct effects of virus infection may result in a range of more predictable endothelial responses, e.g., increased expression of IL-6 and IL-8, modulation (either upregulation or downregulation) in the surface expression of adhesion molecules and endothelial activation antigens (e.g., ICAM-1, E-selectin, VCAM-1, P-selectin, tissue factor, and MHC-I and -II), increased leukocyte adhesion, increases in vascular permeability, suppression of host cell protein synthesis, or induction of apoptosis or necrosis of virally infected endothelium (4, 18, 19, 45, 48). However, none of these responses was observed in our investigation.

There are two significant implications of the results of this investigation. The limited direct effects of hantavirus infection on the function or activation of endothelial cells suggests a more prominent role for immune-mediated effector mechanisms of vascular permeability in HPS and HFRS. The selective activation of the chemokines RANTES and IP-10 provides a mechanism by which hantavirus infection may direct and perhaps enhance the effector immune response to the infected microvascular endothelium.

In addition to the lack of evidence for hantavirus-induced endothelial activation or modulation in CAM or cytokine expression or expression of the hantavirus cellular receptor (CD61), our comprehensive investigation with both SNV and HTN in human renal and lung microvascular endothelial cells revealed no evidence of modulation in the expression of tissue factor or plasminogen activator inhibitor I surface antigens involved in the maintenance of endothelial anticoagulant potentials, no increases in leukocyte adhesion to virally infected endothelial cells, and no attenuation of endothelial host cell protein synthesis (unpublished observations). Furthermore, the ability of hantavirus-infected HMVEC-Ls to form functional permeability barriers and to respond normally to soluble immune mediators of vascular permeability, e.g., TNF-α (Fig. 6), implies that hantavirus infection of the microvascular endothelium may be necessary but insufficient to trigger increases in capillary leakage associated with HFRS or HPS. These results suggest that specific effector immune responses focused at sites of hantavirus-infected vascular tissues may provide the trigger for vascular leakage associated with HPS or HFRS.

The selective induction of the chemokines RANTES and IP-10 in HMVEC-Ls may provide a clue for the involvement of the specific immune response in the pathogenesis of hantavirus-induced vascular diseases. Both RANTES and IP-10 are predominantly chemotactic for mononuclear leukocytes, and IP-10 has been shown to be essential in the development of a protective TH1 response against viral infections in the central nervous system (31). In both HFRS and HPS there is evidence of a TH1-type immune response, characterized by elevated levels of IFN-γ in serum (27, 39). Our data provide an explanation of how such a TH1 immune response could enhance chemotactic signaling and recruitment of activated monocytes and lymphocytes by the hantavirus-infected microvascular endothelium. It has recently been shown that RANTES gene expression in virally infected cells is regulated synergistically by the cooperative binding of IRF-3, IRF-7, and NF-κB p65 nuclear transcription factors at adjacent ISRE and NF-κB bind-

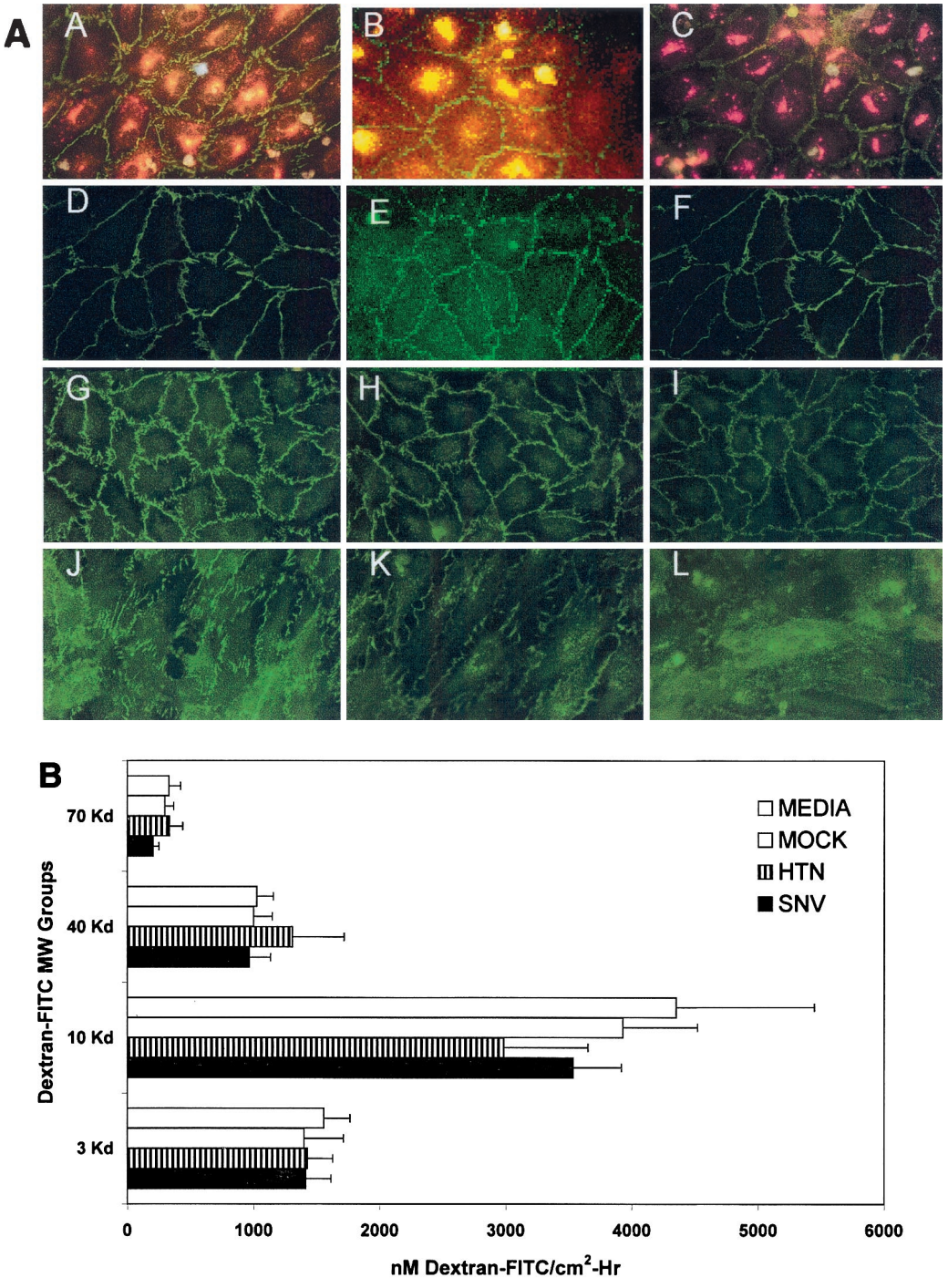

FIG. 6. Effect of hantavirus infection on the establishment and maintenance of functional permeability barriers. (A) Indirect immunofluorescence of the organization and distribution of HMVEC-L junctional integral proteins: ZO-1 in SNV-infected (A), mock-infected (D), uninfected (G), or uninfected TNF-α (24 h)-treated (J) cells; CAD-5 in SNV-infected (B), mock-infected (E), uninfected (H), or uninfected TNF-α (24 h)-treated (K) cells; and CD31 in SNV-infected (C), mock-infected (F), uninfected (I), or uninfected TNF-α (24 h)-treated (L) cells. (B) Measurements of paracellular and transcellular permeability in confluent cultures of SNV-infected, HTN-infected, mock-infected, or uninfected HMVEC-Ls. Fluorescently labeled dextran particles of 10, 40, and 70 kDa were used for paracellular permeability measurements, and 3-kDa dextran particles were used for transcellular permeability measurements, as described in the text. Paracellular permeability was indirectly proportional to the molecular weight of the dextran particles. (C) Measurements of the formation of adherens junctions in uninfected HMVEC-Ls. After experimental disruption by treatment with EDTA, adherens junction complexes in confluent HMVEC-L monolayers were allowed to reform in the presence of complete medium. CAD-5 complexes immunoprecipitated from cell lysates were resolved by SDS-polyacrylamide gel electrophoresis, and the presence of plakoglobin in reformed adherens complexes was determined by Western blotting. (D) Measurements of the reestablishment of functional permeability barriers in confluent cultures of SNV-infected, HTN-infected, mock-infected, or uninfected HMVEC-Ls after experimental disruption of adherens junction complexes by treatment with EDTA.

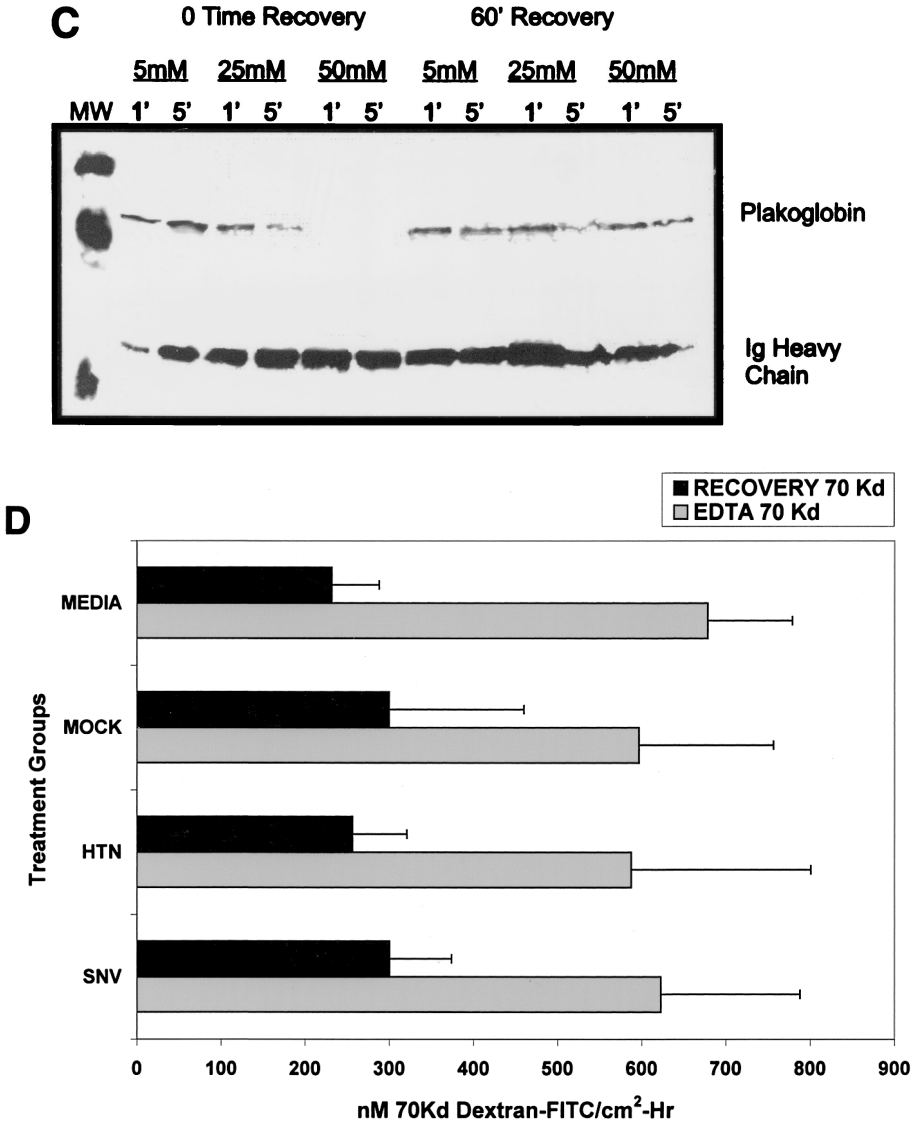

FIG. 6—*Continued.*

ing sites in the RANTES promoter (16). It has also been reported that a similar motif is associated with the regulation of IP-10 gene expression in virally infected astrocytes, which involves binding of transcription factors to ISRE and adjacent NF-κB binding sites in the IP-10 gene promoter (7). Virus infection or treatment with poly(I · C) triggers the phosphorylation and nuclear translocation of IRF-3, which is constitutively present in the cytoplasm of target cells (Fig. 5F). Virus infection or treatment with poly(I · C) triggers the de novo synthesis of IRF-7 and its subsequent nuclear translocation in target cells (35) (Fig. 5G). Both of these events were observed in RANTES- and IP-10-expressing HMVEC-Ls after infection with hantavirus (Fig. 5K and L), indicating their involvement in the observed virally induced chemokine expression by HMVEC-Ls.

Curiously, nuclear translocation of IRF-3 and IRF-7 was observed in HMVEC-Ls in which hantavirus NP was not detected (Fig. 5K and L), suggesting that activation of these transcription factors occurred in uninfected as well as infected HMVEC-Ls. After the initial absorption of virus by the HMVEC-L monolayer in vitro, hantavirus infection spreads from cell to cell. Therefore, one explanation for this observation would be that viral replication preceding viral protein synthesis taking place in newly infected HMVEC-Ls triggers activation of IRF-3 and IRF-7 in the absence of viral NP. Activation of IRF-3 and IRF-7 in NP-negative neighbor cells might also be enhanced by soluble factors expressed by infected cells, e.g., type I interferons (38). In addition to regulation of chemokine gene expression, both IRF-3 and IRF-7 are both involved in the activation of IFN-α/β gene transcription (3, 24, 29, 43); furthermore, type I IFN activates interferon-stimulated gene factor 3, which causes IRF-7 gene induction (42). However, such speculation of the precise mechanisms involved in the direct and indirect effects of hantavirus infection on IRF-3 and IRF-7 signaling in NP-negative HMVEC-Ls can be resolved only with more rigorous experimental examination.

Our study also revealed that the hantavirus-induced chemokine response by HMVEC-Ls was enhanced by the TH1 proinflammatory cytokine, IFN-γ. Other reports have described how the combination of certain proinflammatory cytokines, e.g., IFN-γ and TNF-α, synergistically enhances RANTES gene expression in uninfected endothelial cells through the action and cooperative binding of IRF-1 and NF-κB p65 to ISRE and NF-κB binding elements, respectively, in the RANTES promoter (28, 40). In this investigation we found no evidence for nuclear translocation of IRF-1 or p65 in hantavirus-infected HMVEC-Ls in the absence of IFN-γ (Fig. 5J and M). Although these findings do not preclude hantavirus-induced activities associated with these transcription factors that were not detected in our assays, this result was consistent with our inability to detect virus-specific induction of CAM expression, especially ICAM-1, VCAM-1, or E-selectin gene expression (Fig. 2B to E), which is dependent on NF-κB nuclear transcription factors (8). However, pretreatment of HMVEC-Ls with IFN-γ did result in activation and nuclear translocation of IRF-1 (Fig. 5A). Furthermore, the combination of hantavirus infection plus IFN-γ resulted in the activation and nuclear translocation of NF-κB p65 (Fig. 5N). These findings indicate that under the influence of the TH1 proinflammatory cytokine IFN-γ, activation and nuclear translocation of IRF-1, IRF-3, IRF-7, and NF-κB p65 transcription factors occur in hantavirus-infected microvascular endothelial cells, resulting in the enhanced expression of the chemokines RANTES and IP-10.

These observations can be used to describe a possible scenario for a sequence of events in a pathogenic pathway effecting increased vascular permeability in HFRS and HPS. Infection with hantavirus leads to the generation of antigen-specific activated T cells in primary and secondary lymphoid organs. During this incubation period, viral infection of microvascular endothelial cells results in the expression of modest levels of RANTES and IP-10, attracting activated T cells which home to the postcapillary vascular beds. Antigen-activated infiltrating T cells within the microenvironment express IFN-γ, thus enhancing RANTES expression by the hantavirus-infected microvascular endothelial cells and selectively recruiting more T cells.

This paradigm could also explain the contrasting clinical presentations between HPS and most other cases of adult respiratory distress syndrome (ARDS). Although the pathophysiology of ARDS varies, most cases (especially ARDS secondary to sepsis) are characterized by high levels of proinflammatory cytokines, mononuclear cell and polymorphonuclear neutrophil infiltration, and resulting damage to the pulmonary vascular endothelium (21). However, in HPS cases there is evidence of infiltrating $CD4^+$ and $CD8^+$ T cells with no evidence of infiltrating polymorphonuclear neutrophils or activation and damage to the vascular endothelium of the lung. A recent report has documented findings of increased numbers of T cells producing cytokines, e.g., IFN-γ and TNF-α, in the lungs of HPS victims (36). Our data suggest that hantavirus infection in combination with the proinflammatory cytokine IFN-γ influences the phenotype of infiltrating lymphocytes in the lungs of subjects with HPS. It has been shown that IFN-γ and endothelial cell-derived RANTES selectively induces diapedesis of TH1-type T cells (25). Ennis et al. have described $CD4^+$ and $CD8^+$ T-cell clones with antigenic specificity for the SNV NP (13). These clones were derived from the peripheral blood of donors with documented HPS. One well-characterized $CD8^+$ T-cell clone responded to SNV NP presented by autologous Epstein-Barr virus-transformed B cells by producing IFN-γ but not IL-4. Our studies reveal that MHC-I is richly expressed on hantavirus-infected HMVEC-Ls and is upregulated in the presence of IFN-γ (Fig. 2A). This suggests that hantavirus-infected HMVEC-Ls should be able to competently present SNV antigens to activated antigen-specific T cells. Cognate interaction between hantavirus-specific $CD8^+$ or $CD4^+$ T cells and infected endothelial cells might trigger T-cell activation .

In the setting of hantavirus infection, hantavirus antigen processed and presented by infected endothelial cells might result in the release of soluble immune mediators (e.g., TNF-α) by activated T cells that could trigger the disruption of endothelial intercellular junctions resulting in increases in vascular permeability (Fig. 6A). An investigation of more intimate interactions between HLA-matched immune cells and virally infected HMVEC-Ls would help address these issues. However, these and other questions regarding cellular interactions between the immune system and the hantavirus-infected vascular endothelium await the development of an appropriate animal model.

ACKNOWLEDGMENTS

We thank Deborah Martinson for her excellent technical assistance in cell culture and immunochemistry, Margaret K. Offermann for her advice and review of the manuscript, Mary Renshaw for her expert technical assistance in performing RNA analysis, and Kent Wagoner for his help in the statistical design and measurements employed in this study.

This work was supported in part by a grant from the Centers for Disease Control and Prevention, U50/CCU411374-03-01.

REFERENCES

1. **Anderson, R., S. Wang, C. Osiowy, and A. C. Issekutz.** 1997. Activation of endothelial cells via antibody-enhanced dengue virus infection of peripheral blood monocytes. J. Virol. **71:**4226–4232.
2. **Ansari, A. A., J. B. Sundstrom, H. Runnels, P. Jensen, K. Kanter, A. Mayne, and A. Herskowitz.** 1994. The absence of constitutive and induced expression of critical cell-adhesion molecules on human cardiac myocytes. Its role in transplant rejection. Transplantation **57:**942–949.
3. **Au, W. C., P. A. Moore, D. W. LaFleur, B. Tombal, and P. M. Pitha.** 1998. Characterization of the interferon regulatory factor-7 and its potential role in the transcription activation of interferon A genes. J. Biol. Chem. **273:** 29210–29217.
4. **Avirutnan, P., P. Malasit, B. Seliger, S. Bhakdi, and M. Husmann.** 1998. Dengue virus infection of human endothelial cells leads to chemokine production, complement activation, and apoptosis. J. Immunol. **161:**6338–6346.
5. **Battegay, M., S. Cooper, A. Althage, J. Banziger, H. Hengartner, and R. M. Zinkernagel.** 1991. Quantification of lymphocytic choriomeningitis virus with an immunological focus assay in 24- or 96-well plates. J. Virol. Methods **33:**191–198.
6. **Beck, G. C., B. A. Yard, A. J. Breedijk, K. Van Ackern, and F. J. Van Der Woude.** 1999. Release of CXC-chemokines by human lung microvascular endothelial cells (LMVEC) compared with macrovascular umbilical vein endothelial cells. Clin. Exp. Immunol. **118:**298–303.
7. **Cheng, G., A. S. Nazar, H. S. Shin, P. Vanguri, and M. L. Shin.** 1998. IP-10 gene transcription by virus in astrocytes requires cooperation of ISRE with adjacent κB site but not IRF-1 or viral transcription. J. Interferon Cytokine Res. **18:**987–997.
8. **Collins, T., M. A. Read, A. S. Neish, M. Z. Whitley, D. Thanos, and T. Maniatis.** 1995. Transcriptional regulation of endothelial cell adhesion molecules: NF-kappa B and cytokine-inducible enhancers. FASEB J. **9:**899–909.
9. **Dejana, E.** 1996. Endothelial adherens junctions: implications in the control of vascular permeability and angiogenesis. J. Clin. Investig. **98:**1949–1953.
10. **Dejana, E., M. Corada, and M. G. Lampugnani.** 1995. Endothelial cell-to-cell junctions. FASEB J. **9:**910–918.
11. **Donlon, T. A., A. M. Krensky, M. R. Wallace, F. S. Collins, M. Lovett, and C. Clayberger.** 1990. Localization of a human T-cell-specific gene, RANTES (D17S136E), to chromosome 17q11.2-q12. Genomics **6:**548–553.

12. **Ebnet, K., E. P. Kaldjian, A. O. Anderson, and S. Shaw.** 1996. Orchestrated information transfer underlying leukocyte endothelial interactions. Annu. Rev. Immunol. **14:**155–177.
13. **Ennis, F. A., J. Cruz, C. F. Spiropoulou, D. Waite, C. J. Peters, S. T. Nichol, H. Kariwa, and F. T. Koster.** 1997. Hantavirus pulmonary syndrome: CD8+ and CD4+ cytotoxic T lymphocytes to epitopes on Sin Nombre virus nucleocapsid protein isolated during acute illness. Virology **238:**380–390.
14. **Gavrilovskaya, I. N., E. J. Brown, M. H. Ginsberg, and E. R. Mackow.** 1999. Cellular entry of hantaviruses which cause hemorrhagic fever with renal syndrome is mediated by β3 integrins. J. Virol. **73:**3951–3959.
15. **Gavrilovskaya, I. N., M. Shepley, R. Shaw, M. H. Ginsberg, and E. R. Mackow.** 1998. β3 integrins mediate the cellular entry of hantaviruses that cause respiratory failure. Proc. Natl. Acad. Sci. USA **95:**7074–7079.
16. **Genin, P., M. Algarte, P. Roof, L. Rongtuan, and J. Hiscott.** 2000. Regulation of RANTES chemokine gene expression requires cooperativity between NF-κB and IFN-regulatory factor transcription factors. J. Immunol. **164:** 5352–5361.
17. **Goebeler, M., T. Yoshimura, A. Toksoy, U. Ritter, E. B. Brocker, and R. Gillitzer.** 1997. The chemokine repertoire of human dermal microvascular endothelial cells and its regulation by inflammatory cytokines. J. Investig. Dermatol. **108:**445–451.
18. **Harcourt, B. H., P. A. Rota, K. B. Hummel, W. J. Bellini, and M. K. Offermann.** 1999. Induction of intercellular adhesion molecule 1 gene expression by measles virus in human umbilical vein endothelial cells. J. Med. Virol. **57:**9–16.
19. **Harcourt, B. H., A. Sanchez, and M. K. Offermann.** 1998. Ebola virus inhibits induction of genes by double-stranded RNA in endothelial cells. Virology **252:**179–188.
20. **Harcourt, B. H., A. Sanchez, and M. K. Offermann.** 1999. Ebola virus selectively inhibits responses to interferons, but not to interleukin-1β, in endothelial cells. J. Virol. **73:**3491–3496.
21. **Hasleton, P. S., and T. E. Roberts.** 1999. Adult respiratory distress syndrome—an update. Histopathology **34:**285–294.
22. **Hooper, W. C., D. J. Phillips, M. A. Renshaw, B. L. Evatt, and J. M. Benson.** 1998. The up-regulation of IL-6 and IL-8 in human endothelial cells by activated protein C. J. Immunol. **161:**2567–2573.
23. **Jovov, B., N. K. Wills, and S. A. Lewis.** 1991. A spectroscopic method for assessing confluence of epithelial cell cultures. Am. J. Physiol. **261:**C1196–C1203.
24. **Juang, Y., W. Lowther, M. Kellum, W. C. Au, R. Lin, J. Hiscott, and P. M. Pitha.** 1998. Primary activation of interferon A and interferon B gene transcription by interferon regulatory factor 3. Proc. Natl. Acad. Sci. USA **95:** 9837–9842.
25. **Kawai, T., M. Seki, K. Hiromatsu, J. W. Eastcott, G. F. Watts, M. Sugai, D. J. Smith, S. A. Porcelli, and M. A. Taubman.** 1999. Selective diapedesis of Th1 cells induced by endothelial cell RANTES. J. Immunol. **163:**3269–3278.
26. **Khaiboullina, S. F., D. M. Netski, P. Krumpe, and S. C. St. Jeor.** 2000. Effects of tumor necrosis factor alpha on Sin Nombre virus infection in vitro. J. Virol. **74:**11966–11971.
27. **Krakauer, T., J. W. Leduc, J. C. Morrill, A. O. Anderson, and H. Krakauer.** 1994. Serum levels of alpha and gamma interferons in hemorrhagic fever with renal syndrome. Viral Immunol. **7:**97–101.
28. **Lee, A. H., J. H. Hong, and Y. S. Seo.** 2000. Tumour necrosis factor-alpha and interferon-gamma synergistically activate the RANTES promoter through nuclear factor κB and interferon regulatory factor 1 (IRF-1) transcription factors. Biochem. J. **350:**131–138.
29. **Lin, R., P. Genin, Y. Mamane, and J. Hiscott.** 2000. Selective DNA binding and association with the CREB binding protein coactivator contribute to differential activation of alpha/beta interferon genes by interferon regulatory factors 3 and 7. Mol. Cell. Biol. **20:**6342–6353.
30. **Lin, R., C. Heylbroeck, P. Genin, P. M. Pitha, and J. Hiscott.** 1999. Essential role of interferon regulatory factor 3 in direct activation of RANTES chemokine transcription. Mol. Cell. Biol. **19:**959–966.
31. **Liu, M. T., B. P. Chen, P. Oertel, M. J. Buchmeier, D. Armstrong, T. A. Hamilton, and T. E. Lane.** 2000. The T cell chemoattractant IFN-inducible protein 10 is essential in host defense against viral-induced neurologic disease. J. Immunol. **165:**2327–2330.
32. **Lou, J., J. M. Dayer, G. E. Grau, and D. Burger.** 1996. Direct cell/cell contact with stimulated T lymphocytes induces the expression of cell adhesion molecules and cytokines by human brain microvascular endothelial cells. Eur. J. Immunol. **26:**3107–3113.
33. **Luster, A. D., S. C. Jhanwar, R. S. Chaganti, J. H. Kersey, and J. V. Ravetch.** 1987. Interferon-inducible gene maps to a chromosomal band associated with a (4;11) translocation in acute leukemia cells. Proc. Natl. Acad. Sci. USA **84:**2868–2871.
34. **Majumder, S., L. Z. Zhou, P. Chaturvedi, G. Babcock, S. Aras, and R. M. Ransohoff.** 1998. p48/STAT-1α-containing complexes play a predominant role in induction of IFN-gamma-inducible protein, 10 kDa (IP-10) by IFN-gamma alone or in synergy with TNF-alpha. J. Immunol. **161:**4736–4744.
35. **Mamane, Y., C. Heylbroeck, P. Genin, M. Algarte, M. J. Servant, C. LePage, C. DeLuca, H. Kwon, R. Lin, and J. Hiscott.** 1999. Interferon regulatory factors: the next generation. Gene **237:**1–14.
36. **Mori, M., A. L. Rothman, I. Kurane, J. M. Montoya, K. B. Nolte, J. E. Norman, Waite, D. C., F. T. Koster, and F. A. Ennis.** 1999. High levels of cytokine-producing cells in the lung tissues of patients with fatal hantavirus pulmonary syndrome. J. Infect. Dis. **179:**295–302.
37. **Nichol, S. T., C. F. Spiropoulou, S. Morzunov, P. E. Rollin, T. G. Ksiazek, H. Feldmann, A. Sanchez, J. Childs, S. Zaki, and C. J. Peters.** 1993. Genetic identification of a hantavirus associated with an outbreak of acute respiratory illness. Science **262:**914–917.
38. **Pensiero, M. N., J. B. Sharefkin, C. W. Dieffenbach, and J. Hay.** 1992. Hantaan virus infection of human endothelial cells. J. Virol. **66:**5929–5936.
39. **Peters, C. J., G. L. Simpson, and H. Levy.** 1999. Spectrum of hantavirus infection: hemorrhagic fever with renal syndrome and hantavirus pulmonary syndrome. Annu. Rev. Med. **50:**531–545.
40. **Pine, R.** 1997. Convergence of TNFα and IFNγ signalling pathways through synergistic induction of IRF-1/ISGF-2 is mediated by a composite GAS/κB promoter element. Nucleic Acids Res. **25:**4346–4354.
41. **Salcedo, R., J. H. Resau, D. Halverson, E. A. Hudson, M. Dambach, D. Powell, K. Wasserman, and J. J. Oppenheim.** 2000. Differential expression and responsiveness of chemokine receptors (CXCR1–3) by human microvascular endothelial cells and umbilical vein endothelial cells. FASEB J. **14:**2055–2064.
42. **Sato, M., N. Hata, M. Asagiri, T. Nakaya, T. Taniguchi, and N. Tanaka.** 1998. Positive feedback regulation of type I IFN genes by the IFN-inducible transcription factor IRF-7. FEBS Lett. **441:**106–110.
43. **Sato, M., H. Suemori, N. Hata, M. Asagiri, K. Ogasawara, K. Nakao, T. Nakaya, M. Katsuki, S. Noguchi, N. Tanaka, and T. Taniguchi.** 2000. Distinct and essential roles of transcription factors IRF-3 and IRF-7 in response to viruses for IFN-alpha/beta gene induction. Immunity **13:**539–548.
44. **Shen, J., S. S. To, L. Schrieber, and N. J. King.** 1997. Early E-selectin, VCAM-1, ICAM-1, and late major histocompatibility complex antigen induction on human endothelial cells by flavivirus and comodulation of adhesion molecule expression by immune cytokines. J. Virol. **71:**9323–9332.
45. **Vercellotti, G. M.** 1998. Effects of viral activation of the vessel wall on inflammation and thrombosis. Blood Coagul. Fibrinolysis **9**(Suppl. 2)**:**S3–S6.
46. **Waldman, W. J., D. A. Knight, and E. H. Huang.** 1998. An in vitro model of T cell activation by autologous cytomegalovirus (CMV)-infected human adult endothelial cells: contribution of CMV-enhanced endothelial ICAM-1. J. Immunol. **160:**3143–3151.
47. **Yanagihara, R., and D. J. Silverman.** 1990. Experimental infection of human vascular endothelial cells by pathogenic and nonpathogenic hantaviruses. Arch. Virol. **111:**281–286.
48. **Yang, Z. Y., H. J. Duckers, N. J. Sullivan, A. Sanchez, E. G. Nabel, and G. J. Nabel.** 2000. Identification of the Ebola virus glycoprotein as the main viral determinant of vascular cell cytotoxicity and injury. Nat. Med. **6:**886–889.
49. **Zaki, S. R., P. W. Greer, L. M. Coffield, C. S. Goldsmith, K. B. Nolte, K. Foucar, R. M. Feddersen, R. E. Zumwalt, G. L. Miller, and A. S. Khan.** 1995. Hantavirus pulmonary syndrome. Pathogenesis of an emerging infectious disease. Am. J. Pathol. **146:**552–579.